Tellus (1999), 51A, 588–602
Printed in UK. All rights reserved

TELLUS
ISSN 0280–6495

Rossby wavepacket propagation in a zonally-varying basic flow

By TAKESHI ENOMOTO* and YOSHIHISA MATSUDA, *Department of Earth and Planetary Physics, University of Tokyo, Tokyo, Japan*

(Manuscript received 15 September 1998; in final form 10 May 1999)

ABSTRACT

Rossby wavepacket propagation in a zonally-varying basic flow is examined with a barotropic model in connection with the critical layer. A number of experiments are conducted by systematically changing the longitude of forcing, to analyze interactions between the zonally-varying flow and a Rossby-wave packet. A particular form of wave-activity flux applicable to zonally-varying basic flows is used to illustrate the propagation patterns. Several reflection patterns are found and their mechanism, which is different from those currently proposed, is discussed. The present numerical results show that the wavepacket propagation slows down in the weak wind region and that vorticity anomalies are advected by the anticyclonic basic flow. Vorticity anomalies associated with Rossby waves, in turn, influence the intensity of a subtropical anticyclonic flow in the basic state. The present numerical results are compared with an observed vorticity overturning in the upper troposphere and wave amplification near the jet exit region obtained in a linear numerical study.

1. Introduction

The nonlinear critical layer theory was successfully applied to stratospheric phenomena by McIntyre and Palmer (1983). Vorticity overturnings at the edge of the stratospheric polar vortex resemble that of a time dependent solution for the critical layer of stationary Rossby wave, found by Stewartson (1978), and Warn and Warn (1978), hereafter referred to as the SWW solution. According to the SWW solution, the streamfunction is stationary and forms a cat's eye pattern near the critical latitude, where the basic zonal wind speed becomes zero. Along the cat's eye, the vorticity is passively advected. Associated with the vorticity overturning, the wave absorptivity of the critical layer alternates between absorption and over-reflection, approaching the perfect reflection with time. Irreversible deformation of vorticity contours was named "wave breaking" by McIntyre and Palmer.

It was possible to explain the stratospheric phenomena in the framework of wave braking using the SWW solution as a dynamical model since the stratospheric basic flow is more or less zonally-uniform. On the other hand, it is not evident that "wave breaking" similar to the SWW solution occurs in the upper troposphere, where the zonal variations of the basic flow may not be negligible. It is interesting to examine if the SWW solution is applicable to such tropospheric situations. In addition, Rossby waves observed in the troposphere propagate in the form of a wavepacket rather than a monochromatic wave as assumed in the SWW solution.

The overturnings in the SWW solutions and observed overturnings of PV contours in blocking phenomena (Nakamura, 1994; Nakamura et al.,

* Corresponding author.
Postal address: Sci. bldg. #1, 7-3-1, Hongo, Bunkyo-ku, Tokyo, 113-0033, Japan.
e-mail: eno@geoph.s.u-tokyo.ac.jp.

1997), must be distinguished. Although observed overturnings are shown to be associated with Rossby waves in their study, the "roll-up" patterns are formed due to large wave amplitudes. The numerical experiments by Waugh et al. (1994) showed that large amplitude Rossby waves overturn even without the critical layer. These observational and numerical facts are important in interpreting upper tropospheric phenomena, but these results cannot be directly compared with the critical layer theory. In the present study, the behaviour of small (but not infinitesimal) amplitude waves in a zonally varying flow is considered so that our numerical results can be compared with the SWW solution.

Numerical experiments with wavepacket forcing on a zonally-uniform basic flow were conducted by Waugh et al. (1994). A train of vorticity overturnings in the low-latitudes was simulated in their experiments. Similar experiments were performed by Brunet and Haynes (1996), which clearly demonstrated a low-latitude reflection. A solitary wave solution of Brown and Stewartson (1979) was suggested as a dynamical model for a wavepacket case in Brunet and Haynes. Recently, an asymptotic solution was obtained by Campbell and Maslowe (1998) for a wavepacket case. The asymptotic solution confirmed by linear and nonlinear numerical simulations consists of a train of closed streamlines whose amplitude becomes smaller and less well-defined away from the centre of the wavepacket.

Effects of the zonal variations of basic flow on wave propagation have been considered by several authors. Interhemispheric propagations through a tropical westerly region ("westerly duct") were numerically demonstrated by Webster and Holton (1982). It seems that the behaviour of Rossby waves near the critical latitude was out of their focus so that locations of the forcing which induces a wavepacket propagating toward the tropical easterly region were not systematically changed and low-latitude wave reflection was not discussed either. Webster and Chang (1997) studied a wave propagation in a zonally-varying flow with the emphasis upon energy accumulation in the equatorial westerly region. Wavepacket propagation was examined by Hoskins and Ambrizzi (1993) with a linear model. It was shown in their study that the Rossby-wave refraction toward the regions with large stationary wavenumber is analogous to that of the light wave, as long as the WKB theory is valid. For steady Rossby waves on a zonally-uniform flow with meridional shear, it can be shown that the local steady wavenumber $K_s = \sqrt{\beta_{\text{eff}}/U}$ corresponds to the "refractivity". Here, $\beta_{\text{eff}} = \beta - U_{yy}$ represents the effective beta effect and U the basic zonal flow speed. It is, however, unclear to what extent this explanation can apply to a zonally-varying flow.

In the present study, numerical experiments are systematically conducted with both linear and nonlinear models in order to examine Rossby-wave propagation in a zonally-varying flow, especially near the critical line. Interactions between a zonally-varying flow and a Rossby wavepacket are discussed in Section 3. In Section 4, a new mechanism of reflection in a zonally-varying basic flow is proposed and intensity fluctuations of the subtropical high are discussed. Further, the present results are compared with other observational and numerical studies. Firstly, implications of the present results for an observed vorticity overturnings detected by Postel and Hitchman (1999) are discussed. Secondly, the results of Naoe et al. (1997) are reexamined to identify mechanisms for reflection in the jet and the wave amplification in the jet exit region.

2. Model description

A spectral, barotropic model on a sphere is used in the present study. The absolute vorticity equation,

$$\frac{\mathrm{d}q}{\mathrm{d}t} = fD + \nu\nabla^4\zeta' \tag{1}$$

is numerically integrated. Here, q is the absolute vorticity, ζ' the perturbation relative vorticity, D the divergence, and ν the hyper-diffusion coefficient. The first term on the right hand side of eq. (1) represents a vorticity forcing. In all the present experiments, the forcing is implemented by a circular region of vorticity divergence with the radius of about 1500 km. The nondimensional forcing amplitude is set $D^* = 0.05$. The parameter D^* is defined in

$$D = D^* d, \tag{2}$$

where d^{-1} is a characteristic time scale of the forcing. The parameter d can be defined by

$$d = U/L, \tag{3}$$

where U is a characteristic zonal wind speed near

the forcing and L the wavelength of the steady Rossby wave induced by forcing. Biharmonic diffusion, represented in the second term on the right hand side of eq. (1), is included in the present model to eliminate grid-scale noise. The value of the biharmonic diffusion coefficient $\nu = 3 \times 10^{15}$ m^4/s means that the amplitude of the smallest scale decreases by e^{-1} every 1/8 of a day. No other dissipative effects are included in the model. The zonal and total truncation wavenumbers of our model are 21 and 85, respectively (M21N85). In preliminary experiments with zonally uniform basic state, a train of vorticity overturnings is reproduced, which is also found in previous studies (Brunet and Haynes, 1996; Waugh et al., 1994.) In addition, no transient waves originated by barotropic instability, which requires a fine zonal resolution, are found. Therefore it seems that an M21N85 model is adequate for the present study. The authors conducted a study on the meridional resolution necessary for correct representation of both the inviscid and viscous Rossby-wave critical layers; this study will be reported elsewhere (Enomoto and Matsuda, 1999). The wave amplitude used in the present study corresponds to the one used in the weakest case of Waugh et al. (1994) so that nonlinear terms are small and meridional wave propagation is possible except near the critical line.

The basic zonal flow consists of the zonally-uniform and zonally-varying components,

$$u_0(\lambda, \phi) = \bar{u}_0(\phi) + \varepsilon \tilde{u}_0(\lambda, \phi). \tag{4}$$

The subscript 0 denotes the basic state. The zonally-uniform basic wind field $\bar{u}_0(\phi)$, taken from Waugh et al. (1994), mimics that in the upper troposphere:

$$\bar{u}_0(\phi) = a \cos \phi + b \sin 2\phi + c \sin^2 2\phi, \tag{5}$$

where $a = -5$, $b = 2.5$, $c = 32$ m/s. The zonally-varying component $\tilde{u}_0(\lambda, \phi)$ that includes the zonal wavenumber 1 component is identical to the one assumed in Naoe et al. (1997).

$$\tilde{u}_0(\lambda, \phi) = (\bar{u}_0(\phi) - u_c) \cos^2 \phi \cos \lambda, \tag{6}$$

where

$$u_c = \frac{\int_0^{\pi/2} \bar{u}_0(\phi) \cos^2 \phi \, d\phi}{\int_0^{\pi/2} \cos^2 \phi \, d\phi} = \frac{4}{\pi} \int_0^{\pi/2} \bar{u}_0(\phi) \cos^2 \phi \, d\phi. \tag{7}$$

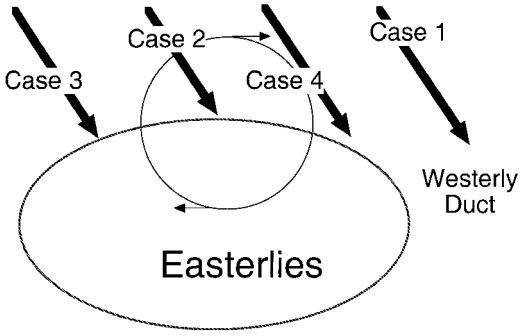

Fig. 1. Schematic diagram representing the configuration of our experiments. The basic flow is easterly within the oval and westerly outside. The circle with two thin arrows represents a NH subtropical high associated with the basic flow. Thick arrows represent Rossby wavepacket propagation.

The basic state is assumed to be independent of time. Note that the linear model includes advection by this zonally-varying component. The zonally-uniform component of the basic state in Naoe et al. was used only for reexamination of their results (Section 4), because its jet is too concentrated to allow Rossby waves to propagate meridionally. For the degree of the zonal variations, $\varepsilon = 1$ is assumed throughout the present study. That value corresponds to the weakest zonal variation in Naoe et al.

Fig. 1 shows a schematic experiment configuration. The westerlies predominate in the extratropics and the easterlies are confined within a longitudinal sector in the tropics. The other tropical regions are covered with the westerlies, which act as a westerly duct for stationary Rossby waves. The basic state with the zonal asymmetries means longitudinal variations in the zonal wind speeds associated with meridional flows. It should be noted that the centre of the subtropical high is on the meridian where the meridional shear takes its maximum value since the zonally-varying component of the basic state $\tilde{u}_0(\lambda, \phi)$ is westerly on the extratropical side and easterly on the tropical side.

3. Results

A series of experiments was conducted to examine interactions between the subtropical high and a Rossby wavepacket by changing the position of

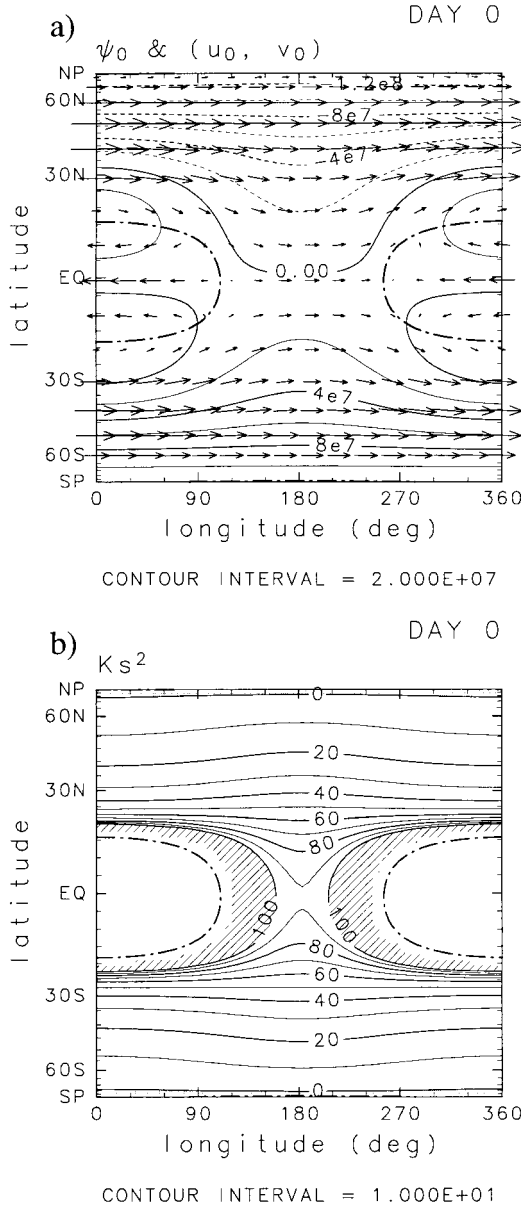

Fig. 2. (a) Distribution of the basic streamfunction and velocity fields defined by eqs. (4)–(7) for case 1. Positive and negative contours of the streamfunction are represented by solid and broken lines, respectively. The dot-dashed line in the tropics corresponds to the line of $u_0 = 0$. (b) Corresponding distribution of stationary Rossby wavenumber, K_s^2. See the text for the definition of K_s. Regions with $K_s^2 \leqslant 0$ are shaded and those with $K_s > 10$ are hatched, excluding the easterly region. The basic states for other cases are obtained by a translation of this basic state in the zonal direction.

the forcing. The results are classified into four representative cases, as shown in this section. In case 1, an interhemispheric wave propagation takes place. In case 2, a wavepacket reaches the critical line in the region with a maximum meridional shear of the basic zonal winds. In that region, the basic flow is comparably zonally-uniform. In cases 3 and 4, a wavepacket reaches the exit and entrance of the tropical easterlies, respectively. Note that instead of changing the position of the forcing region, the centre of the subtropical high λ_C is varied in this study. The centre of forcing is fixed at 40°N, 90°E in all the experiments shown in this section.

3.1. *Case 1*

Fig. 2a shows a horizontal distribution of the basic streamfunction and velocity fields. Note that the ordinate is scaled with the sine of latitude to emphasize features in the low-latitudes. The maximum zonal velocity in the westerly duct located at 180°E, is about 10 m/s. The distribution of the steady Rossby wavenumber K_s corresponding to u_0 in Fig. 2a is shown in Fig. 2b. The wave with the zonal wavenumber k is reflected at the turning latitude, where $K_s^2 = k^2$. In shaded regions with $K_s^2 \leqslant 0$, propagation with any wavenumbers is impossible. In Fig. 2a, the turning latitudes for long waves are located poleward of 60°N only, implying that both northward and southward propagations are possible. A hatched region with $K_s > 10$ surrounds the critical line. All waves are refracted toward this region and the wave activity is eventually accumulated in this "black hole", according to the propagation theory with the WKB approximation (see Hoskins and Ambrizzi, 1993 and references therein).

Fig. 3a shows perturbation streamfunction ψ' field associated with a Rossby-wave meridional propagation at day 14. One of wavetrains emanating from the source region propagates northeastward and finally reach the critical line near 15°N, 270°E after reflected southeastward at the turning latitudes near 70°N, 135°E. The other propagates southeastward from the forcing region into southern hemisphere midlatitudes through the westerly duct. An appropriate wave-activity flux may illustrate this interhemispheric propagation in a zonally-varying flow more intuitively.

In this study, a new formulation of wave-activity

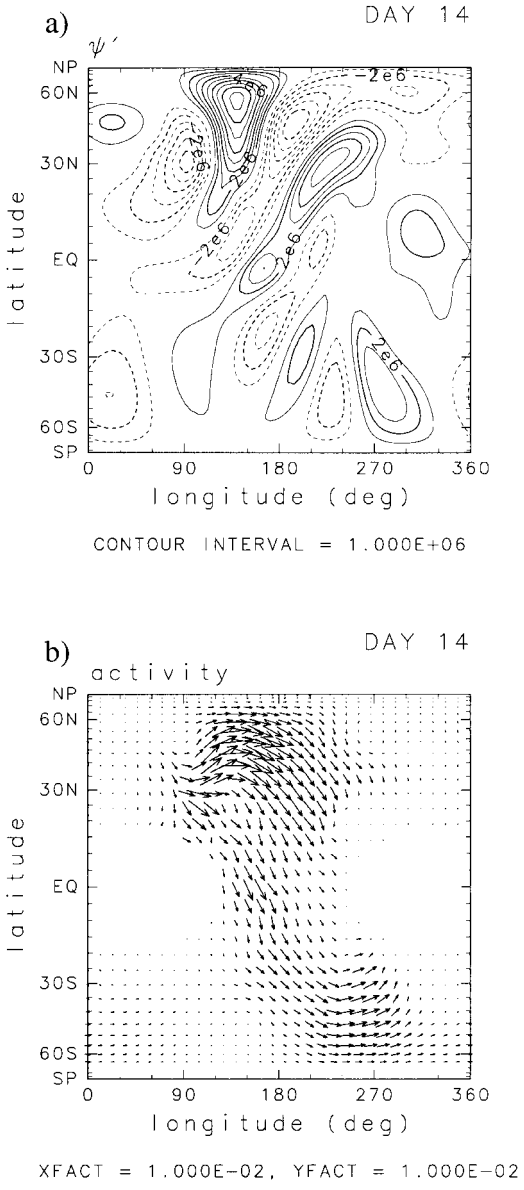

Fig. 3. Distribution of (a) the perturbation streamfunction field and (b) the corresponding wave-activity flux at day 14 for case 1. Positive and negative contours of the streamfunction are represented by solid and broken lines, respectively. See the text for the definition of wave-activity flux.

flux proposed by Takaya and Nakamura (1997) is adopted. This flux can visualize a snapshot of wave propagation in a zonally-varying field without phase dependency. Moreover, the flux is parallel to the local group velocity of stationary Rossby waves. For the present barotropic model, the equation of the wave-activity conservation is written as

$$\frac{\partial M}{\partial t} + \nabla \cdot \boldsymbol{W} = S, \tag{8}$$

where the wave-activity pseudomomentum (M) and its flux ($\boldsymbol{W}$) are defined as

$$M = \frac{1}{4}\left(\frac{q'^2}{|\nabla q_0|} + \frac{u'^2 + v'^2}{|\boldsymbol{u}_0|}\right)\cos\phi \tag{9}$$

and

$$\boldsymbol{W} = \frac{1}{2|\boldsymbol{u}_0|}\begin{bmatrix} u_0\left(v'^2 - \dfrac{\psi'}{a\cos\phi}\dfrac{\partial v'}{\partial\lambda}\right) \\ \qquad - v_0\left(u'v' + \dfrac{\psi'}{a}\dfrac{\partial v'}{\partial\phi}\right) \\ u_0\left(-u'v' + \dfrac{\psi'}{a\cos\phi}\dfrac{\partial u'}{\partial\lambda}\right) \\ \qquad + v_0\left(u'^2 + \dfrac{\psi'}{a}\dfrac{\partial u'}{\partial\phi}\right) \end{bmatrix}\cos\phi, \tag{10}$$

respectively, and S represents the source/sink term. The wave-activity flux defined in McIntyre and Shepherd (1987) is exact even for finite amplitude waves so that it is applicable even near the critical line, but strong phase dependency remains because it is based on pseudoenergy. The wave-activity flux based on Plumb (1985) is phase independent, but a zonally-uniform basic flow must be assumed. Although the wave-activity flux proposed by Takaya and Nakamura cannot properly represent the Rossby-wave behaviour near the critical line, this flux has advantages in representing wave-activity propagation in a zonally-varying basic state without phase dependency.

A latitude–longitude distribution of the wave-activity flux at day 14 is shown in Fig. 3b. The wave-activity flux across the equator indicates an interhemispheric propagation. The flux is convergent along in the fringe of the tropical easterly region with large K_s, where the wave-activity take-off tends to be accumulated (Webster and Chang, 1997 and the references therein). The waves

reflected at higher latitudes of the northern hemisphere also converge into the subtropics. Similarly, the waves entering into the southern hemisphere are reflected at the turning latitudes and finally absorbed into the subtropics. These propagation characteristics in the southern hemisphere midlatitudes are clearly visualized with this flux.

3.2. *Case 2*

In case 2, a wavepacket reaches the critical layer in a region near λ_C. The contours of basic streamfunction run locally parallel to the latitude circles. The waves are reflected back to the midlatitudes by a mechanism similar to the SWW solution. Fig. 4 illustrates the time evolution of the ψ' and ζ' fields at day 7, 14, and 21. At day 7, the ψ' field indicates northeastward and southeastward wave propagations from the source. The wavetrain propagating northeastward reaches the turning latitudes and then it is reflected back toward the lower latitudes. At day 14, a single wavetrain remains in the ψ' field. Cyclonic anomalies centred at 33°N, 170°E with the NW–SE phase tilt are indicative of a reflection in the subtropics. The ψ' anomalies between the forcing and $\sim$180°E are associated mostly with reflecting waves. Farther to the east, the reflecting waves appear to be superposed on the wavetrain that propagated northeastward directly from the forcing region.

The time evolution in ζ' reveals mechanisms of the reflection more clearly. The amplitude of ζ' anomalies is larger in the tropics than in the midlatitudes since the meridional wavenumber becomes large near the critical layer. A pair of intense ζ' anomalies that straddle the critical line rotate anticyclonically. Associated with this rotation, the tilt of the phase lines changes from NE–SW to NW–SE by day 14. As a result, a reflection occurs. The absolute vorticity also over-

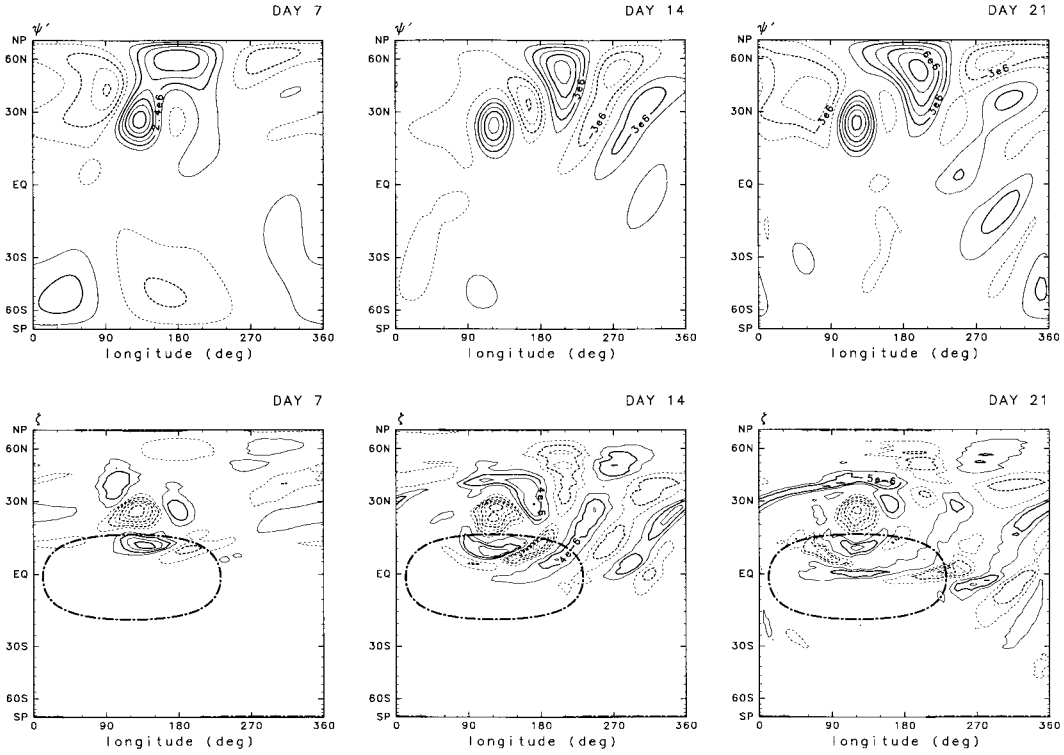

Fig. 4. Time evolution of the perturbation streamfunction (upper panels) and perturbation relative vorticity (lower panels) fields at day 7, 14, and 21 for case 2. Broken lines represent negative contours. Dot-dashed curves in the lower panels represent contours with $u_0 = 0$.

turns in association with this rotation (not shown). At day 21, negative ζ' anomalies near the critical line become stagnant and act to steadily enhance anticyclonic flow in the basic state. A stagnation of ζ' anomalies can be one of possible mechanisms that causes fluctuations in the strength of the subtropical high in the basic state. The low-latitude wave reflection in Fig. 4 can be confirmed in Fig. 5, where the wave-activity accumulated near 20°N, 120°E is reflected back polewards.

The rotating vorticity anomalies around the critical line are reminiscent of the SWW solution. It might be tempting to interpret that the reflection occurring in the present experiment is associated with nonlinear wave breaking as in the SWW solution. The linear experiments shown in Fig. 6, however, reproduce a ψ' field at day 14 very similar to that in Fig. 4. Under the assumption of the SWW solution, the meridional vorticity advection is due to the wave induced meridional flows, which are as important as the basic zonal flows in the critical layer. In our linear model, in place of the wave induced flows, the anticyclonic flow of the basic state advects ζ' anomalies. In other words, the subtropical high plays the role of the cat's eye in the SWW solution. Note that in the present linear model, interactions between the zonally-varying basic state with $k=1$ and the disturbances are included while interactions among higher harmonics of the disturbances are omitted. The reflection reproduced with our linear model suggests that the singularities associated with the critical layer may be removed not by nonlinearity or viscosity but by the zonal variations of the basic flow as previously discussed by Merkine and Bar-Server (1989) for idealized blocking flows.

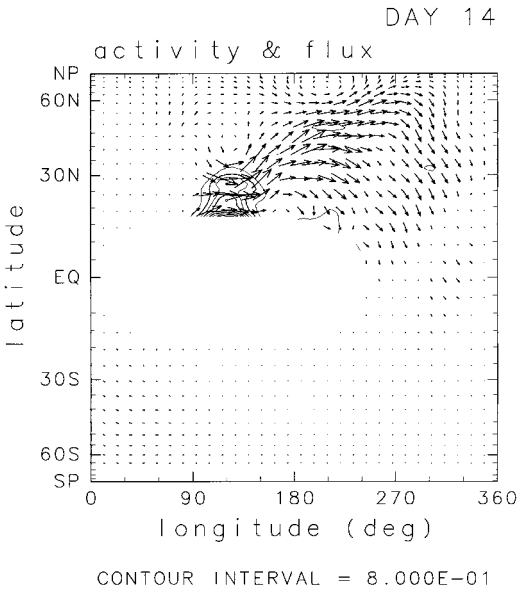

Fig. 5. Distribution of wave-activity (contours) and its flux (arrows) at day 14 for case 2.

3.3. *Case 3*

In case 3, the centre of the subtropical high is located at 180°E on the equator so that the wave forced near 40°N, 90°E approaches this region from the northwestern side. Fig. 7 shows the time evolution of ψ' and ζ' fields at day 7, 14, and 21. The perturbations are still confined in the northern hemisphere even at day 14, which implies a low-latitude reflection. A southeastward wavepacket propagation is apparent in the ψ' field at day 7, consistent with the NE–SW tilt of ψ' anomalies. At day 14, the incident and reflected wavetrains are found in the ζ' field. This vorticity pattern is indicative of a reflection at $\sim$180°E.

The reflection can occur at a turning latitude, but it is clear from Fig. 2b that there are no turning latitudes in the subtropics, rather K_s is positive and large there. It seems that the ζ' anomalies are advected by the anticyclonic flow so that their phase lines change their direction, resulting in a reflection. The phase lines exhibit a NE–SW tilt on the western side and a NW–SE tilt on the eastern side. Around 23°N, 180°E, the phase lines are almost zonal, suggesting that the reflection occurs along this meridian. In contrast to case 2, the reflection occurs slightly ($\sim$8°) north of the critical line (15°N). This also suggests that nonlinear effects are small. Actually, the results in the linear model are quite similar to those in the nonlinear model (not shown). Another interesting feature in Fig. 7 is stagnated positive ζ' anomalies in the northern flank of the anticyclonic basic flow (25°N, 180°E). These anomalies act to weaken this anticyclonic flow.

A wave-activity flux and its divergence at day 14 shown in Fig. 8a clearly demonstrate that the flux is convergent to the west and divergent to the east of the 180°E meridian, respectively. The convergence and divergence indicate absorption and

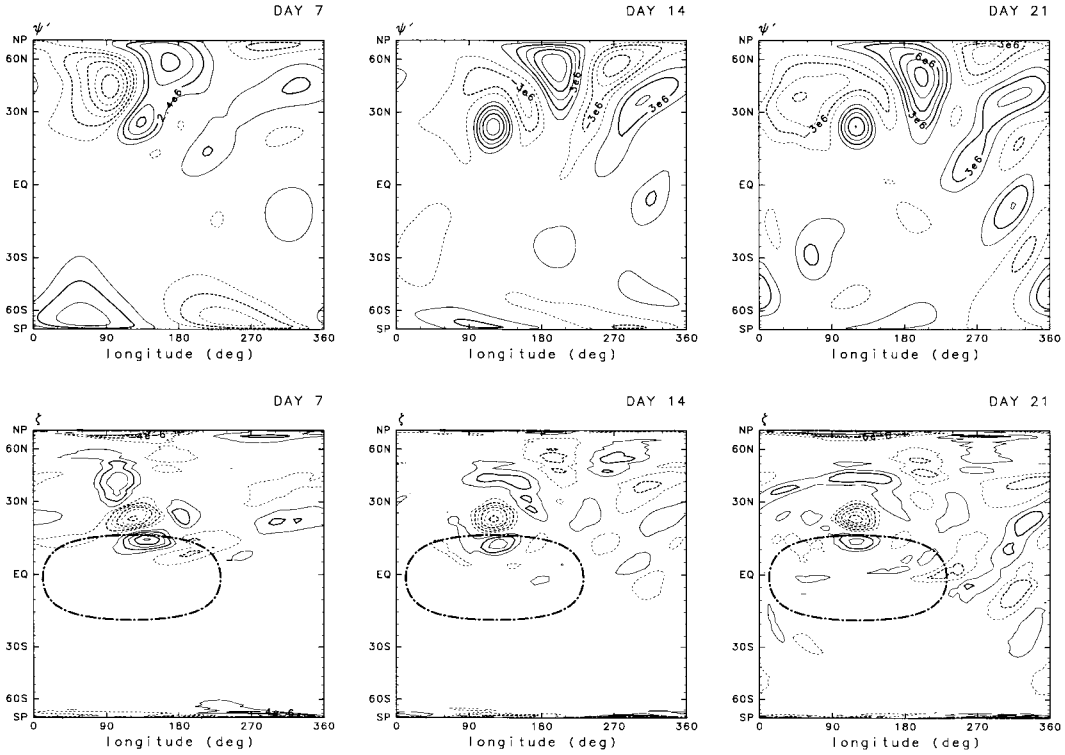

Fig. 6. As in Fig. 4 except for the results with the linear model for case 2.

over-reflection of the wave-activity, respectively. Waves seem to be amplified near the jet exit, which is also found in the experiments of Naoe et al. (1997). The divergence of the wave activity flux contributes to this amplification.

To understand the wave amplification more clearly, a distribution of barotropic KE (kinetic energy) conversion $-u'v'a^{-1}\partial u_0/\partial\phi$ is shown in Fig. 8b. The other component of barotropic KE conversion $-(u'^2-v'^2)(a\cos\phi)^{-1}\partial u_0/\partial\lambda$ is found to be much smaller in our experiment. Naoe et al. calculated growth rates of barotropic instability for their basic state and found that barotropic instability is very small. Their result suggests that the barotropic instability is negligible for our basic state whose jet is less concentrated than theirs. In fact, no significant transient anomalies are found in our experiments. The conversion of basic flow energy into disturbance energy is found to occur near 30°N, 270°E, to the east of the anticyclonic flow, where the meridional flow is equatorward. Meanwhile, the phase lines run in the NW–SE direction in this region, as in both fields at day 14 and 21 in Fig. 7. Although the meridional shear is weaker, a strong negative correlation between u' and v' on the southern flank of the jet results in the conversion from the basic flow energy into disturbance energy there.

3.4. *Case 4*

In Case 4, a wavepacket is directed toward the entrance of the tropical easterly jet. The centre of the subtropical high is located at 60°E on the equator. In this case, also, an important role of advection by the zonally-varying basic flow is demonstrated as follows.

Fig. 9a shows distribution of ζ' at day 14. A wavetrain is found to propagate in the westerly duct. A more striking feature is that the ζ' anomalies trapped in the easterly entrance region are advected westward for several days in the easterly region, where the stationary waves cannot exist in the linear theory. After advected across these

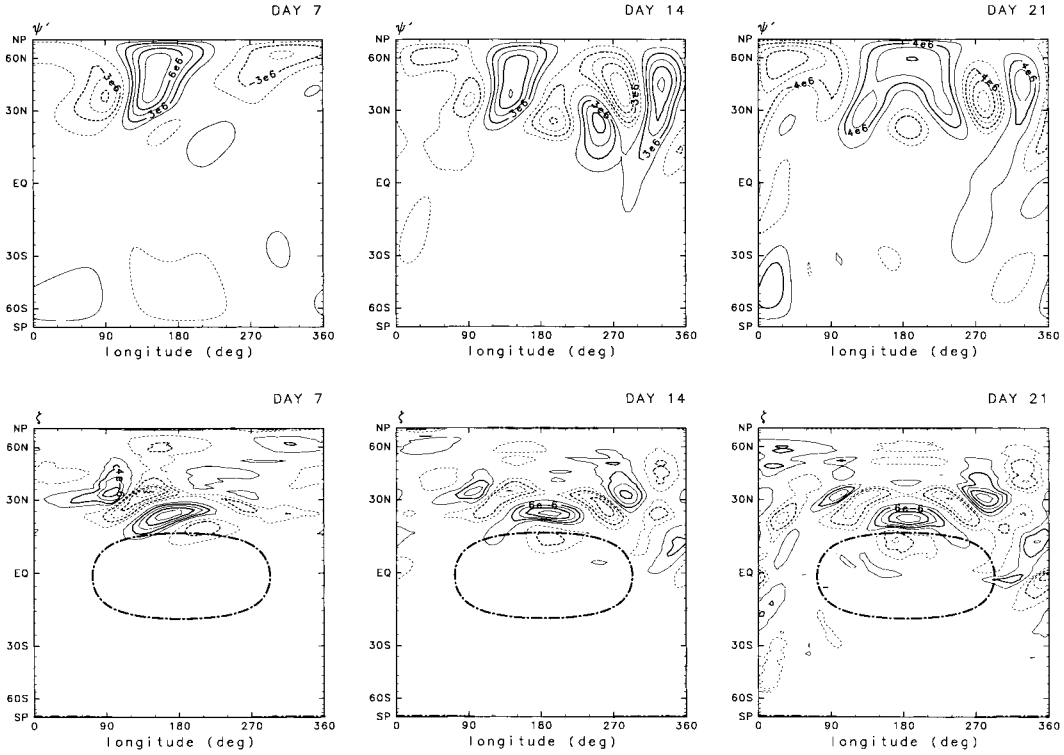

Fig. 7. As in Fig. 4 except for case 3.

easterly region, the ζ' anomalies reach the entrance of the westerly region, and these anomalies begin to propagate again northeastward. Positive and negative anomalies are bent near 0°N, 5°E and 7°N, 7°E, respectively. These anomalies and those near 30°N, 60°E form a northeastward wavetrain. This northeastward propagation is manifested in the phase line of ζ' anomalies with a NW–SE tilt. The corresponding distribution of wave activity and its flux in Fig. 9b clearly exhibit the northeastward emanation of the wave activity towards the westerly jet from the southern edge of its entrance. Emanation from the packet near 20°N, 15°E is confirmed by northeastward flux. This emanation region may be regarded as the secondary source that emerges to the west of the forcing region.

4. Summary and discussion

In this section, the results of the four cases shown in the previous section and other additional cases are summarized. Absorption–reflection behaviour of wave activity and associated fluctuations of intensity of the subtropical high are discussed. Finally, the results of the present study are compared with other observational and numerical studies.

4.1. Reflection in a zonally-varying flow

Low-latitude reflection occurs in all the experiments but for case 1, where an interhemispheric propagation is realized. Fig. 10 shows a schematic diagram for summarizing various reflection patterns realized in the experiments. In case 2, SWW-like reflection occurs, during which a pair of vorticity anomalies rotate around the critical line to the north of the centre of the basic-state subtropical high. In case 3, the vorticity distribution is characterized by the change in the orientation of the phase lines of anomalies from NE–SW to NW–SE that results from the advection by the anticyclone. In case 4, part of wave energy associated with a wave train propagates into the

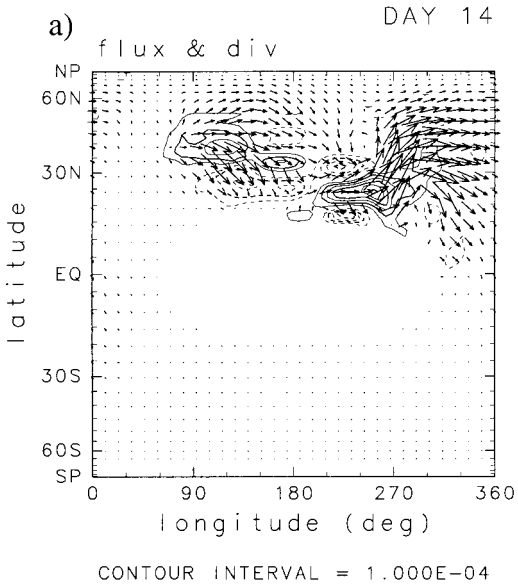

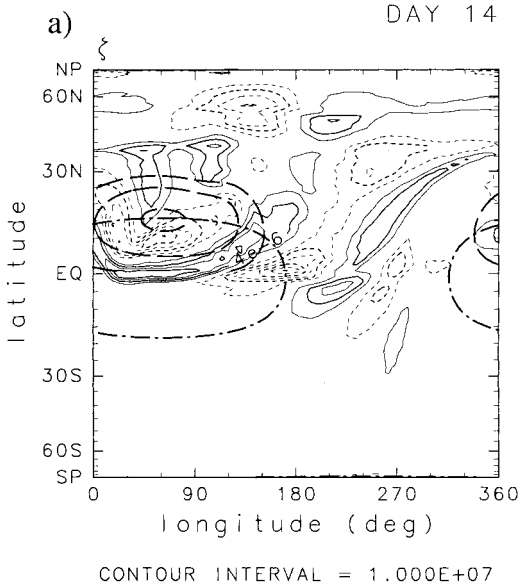

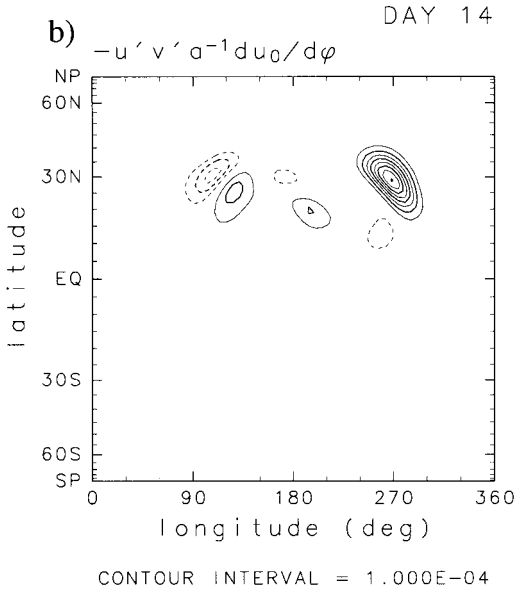

Fig. 8. Distribution of (a) the wave-activity flux (arrows) and its divergence (contours) and (b) barotropic KE conversion $-u'v'a^{-1}\partial\bar{u}_0/\partial\phi$ at day 14 for case 3. Solid (broken) lines in (a) and (b) represent positive (negative) contours of wave-activity flux divergence and barotropic conversion, respectively.

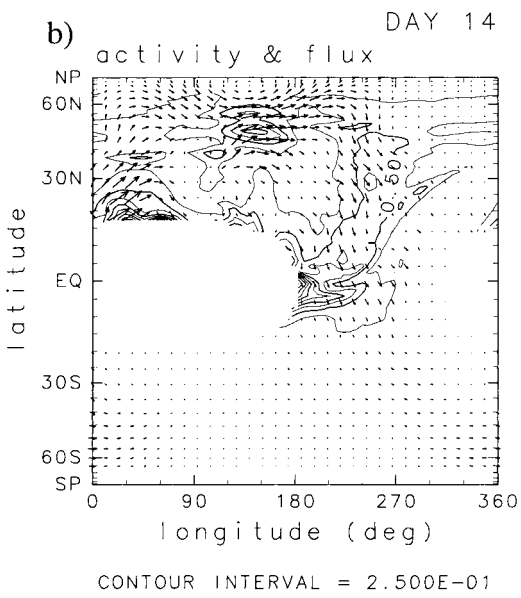

Fig. 9. (a) Distribution of the perturbation relative vorticity at day 14 for case 4. Broken lines represent negative contours. The line of $u_0 = 0$ is denoted by a dot-dashed curve in the tropics. Contours of the streamfunction that represent the NH subtropical anticyclonic flow are denoted by thick broken lines. (b) Distribution of the wave-activity (contours) and its flux (arrows).

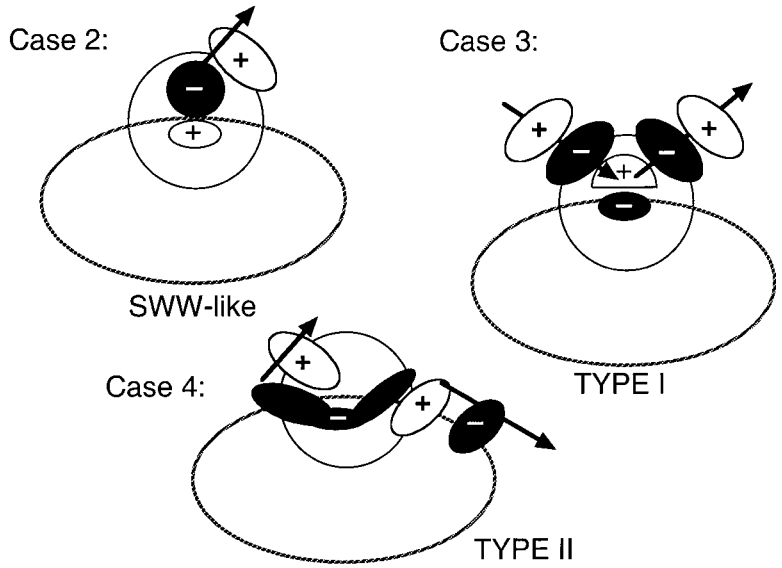

Fig. 10. Schematic reflection patterns in a zonally-varying flow. The large oval and circle are as in Fig. 1. Closed lines with positive and negative signs represent vorticity anomalies. A wavepacket propagates in the direction of arrow.

southern hemisphere through the westerly duct, and the rest is advected by the basic-state easterlies with no emanation of wave activity. Only after the vorticity anomalies reenter the westerly jet from its entrance, north-eastward propagation of wave activity occurred. Henceforth the vorticity evolution patterns similar to cases 3 and 4 are referred to as type I and II, respectively. Vorticity patterns of some experiments other than the four cases are classified into these types as in Table 1. It should be noted that in all three cases (case 2, 3, and 4), vorticity is advected, not by the wave-induced flow near the critical line, but by the anticyclonic flow associated with zonal variations of the basic flow.

Table 1. *Variation of the magnitude of fluctuations in the subtropical high and type of vorticity distribution for experiments with various values of λ_C: see the text for the definitions of λ_C and $\Delta\psi$*

λ_C(°E)	$\Delta\psi$ ($\times 10^6$ m^2/s)	Type of vorticity distribution
0	0	interhemispheric propagation
60	2	II
90	6	SWW-like (and II)
120	7	SWW-like (and II)
150	−2	I (and II)
180	−4	I

The mechanism of wave reflection described above, differs from the mechanism at turning latitudes or from that described by the SWW solution. In the present basic field, the subtropical jet is not concentrated and the value of effective beta in the southern flank of the jet is rather large, thus turning latitudes that may cause wave reflection are not present there. It is demonstrated in the present numerical study that low-latitude reflection can occur as a change of the direction of the phase lines due to the zonally-varying basic flow, even in the linear model. The basic flow in the present study is composed of the zonally-uniform and zonally-varying components as stated in eq. (4). The former component corresponds to a zonal mean flow with meridional shear shown in eq. (5) while the latter component shown in eq. (6) corresponds to a subtropical anticyclonic flow. In the lower latitudes where the zonal mean flow is weak ($\bar{u}_0 \approx 0$) the zonally-varying component $\tilde{u}_0$ mainly advects vorticity anomalies. Thus,

time evolution of vorticity in our linear model in the regions with $\bar{u}_0 \approx 0$ is described by,

$$\frac{\partial q}{\partial t} = -\varepsilon \left(\tilde{u}_0 \frac{\partial}{\partial x} + \tilde{v}_0 \frac{\partial}{\partial y} \right) q, \tag{11}$$

where ε is the degree of the zonal variations and the tilde denotes the zonally-varying part of the basic flow. The stationary wavenumber for a zonally-varying basic flow is,

$$K_s^2 = \beta_{\text{eff}}/U, \tag{12}$$

where

$$\beta_{\text{eff}} = \beta - U_{yy}, \qquad U = \bar{u}_0 + \varepsilon \left(\tilde{u}_0 + \frac{l}{k} \tilde{v}_0 \right),$$

under the WKB approximation. Even at the critical latitude $\bar{u}_0 = 0$, the K_s remains finite. The singularities may be removed as stated above without nonlinear and/or viscous terms (Merkine et al., 1989). The value of u_0 becomes small only at the entrance and exit of easterly regions and the centre of the subtropical high. This result contrasts with the fact that advection by the wave-induced flow becomes important in the SWW solution. The time evolution of vorticity in the SWW solution is described by,

$$\frac{\partial q}{\partial t} = -\left(u_0(y) \frac{\partial}{\partial x} + \delta v' \frac{\partial}{\partial y} \right) q. \tag{13}$$

The perturbational meridional velocity v' (prime denotes the departure from the basic state and δ the wave amplitude) is associated with waves and of primary importance in absorption–reflection behaviour, since the absorptivity α may be defined by the zonal average of eq. (13) as

$$\alpha \equiv \frac{\partial \bar{q}}{\partial t} = -\delta^2 \frac{\partial}{\partial y} \overline{v'q'}. \tag{14}$$

The present numerical results raise a question on the applicability of the SWW solution to a zonally-varying basic flow in the upper troposphere. It is shown that wave-packet propagation and reflection in a zonally-varying basic flow can be sufficiently described as linear processes. Then, the use of a linear model, as in Hoskins and Ambrizzi and Naoe et al. may be justified if the zonally-varying component is important in the reflection mechanism. It will be further discussed in Subsection 4.4 whether or not the mechanism of reflection shown in Naoe et al. is the same, as that in the present experiments.

4.2. *Stagnant anomaly and intensity fluctuations of subtropical high*

Experiments other than the four cases discussed in the previous section were conducted to examine effects of Rossby wavepacket propagation on the intensity of subtropical high by changing the longitude of its centre λ_C. Table 1 summarizes the results, including the 4 cases discussed above. The first column indicates λ_C in the assumed basic flow. The second column shows the change of the circulation intensity $\Delta\psi$, defined as the difference between the final and initial values of the streamfunction at the centre of the anticyclonic flow. The type of time evolution of the anomalies is shown in the third column for reference.

In case 2, negative vorticity anomalies (centred near 25°N, 120°E at day 14 in Fig. 4) become stagnant and strengthen the anticyclonic flow associated in the basic state. In case 3, positive vorticity anomalies (centred near 25°N, 190°E at day 14 in Fig. 7) become stationary and weaken the anticyclonic circulation. It should be noted that, when the sign of the vorticity forcing is changed from positive to negative, the result remains the same except for the sign reversal in the perturbation streamfunction and vorticity fields (not shown). This result indicates that the reflection processes are essentially linear. There are vorticity anomalies adjacent to the stagnant anomalies with an opposite sign (10°N, 120°E in Fig. 4 and 15°N, 190°E in Fig. 7). These anomalies are much weaker than the stagnant anomalies and supposed to be evanescent in the easterlies. The stagnant anomalies, by contrast, maintain its amplitude. The superposition of incident and reflecting waves probably contributes to the maintenance of the wave amplitude and stagnation.

4.3. *Implications for the overturnings detected by Postel and Hitchman*

Recently, large-scale overturnings of potential vorticity contours in the upper troposphere were found by Postel and Hitchman (1999; hereafter referred to as PH). In their data analysis, frequent occurrences of these phenomena were confined to the subtropical ocean, where the ambient winds are weak. It was further argued that the overturnings were associated with the upstream subtropical high. It seems that there are some features

common between the present numerical results and those of PH. It has been found in the present numerical results that in a weak-wind region, the zonally-varying component becomes dominant and acts to advect vorticity anomalies associated with an incident Rossby wavepacket. It was shown in PH that the overturnings were associated with the vorticity advection. In Fig. 8 of PH, it is shown that a part of the wavepacket propagating in the tropical westerly duct enters the easterly region and is advected westward. This vorticity pattern is similar to that of Fig. 9a (case 4). Vorticity anomalies may be associated with a Rossby wavepacket excited over the Himalayas. The wavepacket may propagate southeastward and then interact with the monsoon high. In case 4 of the present study, the wave source is similarly located north of the centre of the basic-state anticyclonic flow. It is unclear whether wave-activity advected by the basic anticyclonic flow across the easterlies reenters the westerlies and emanates from the region to the west of the original source in Fig. 8 of PH. If wave-activity flux proposed by Takaya and Nakamura (1997) was estimated from the data, the mechanism for the vorticity overturnings could be clarified.

4.4. *Wavepacket propagation in a concentrated jet used in Naoe et al. (1997)*

Naoe et al. (1997) thoroughly examined effects of a zonally-varying jet stream wave-guide on Rossby-wave propagation. In their experiments, a wavepacket, which is forced near the jet entrance region, propagated zonally along the jet. It seems that low-latitude reflection is out of scope of their study. The same basic state is reproduced in Fig. 11a. The region with negative K_s^2 southward of the jet shown in Fig. 11b reveals the existence of the turning latitudes near the equator, which work as a possible "reflector". Experiments were conducted to reexamine the results of Naoe et al. (1997) in comparison with case 3. This case is chosen because a wavepacket is forced in the jet entrance region, as in the cases of Naoe et al. (1997). The centre of the forcing is located at 30°N, 90°E, and $\lambda_C = 180°$E.

The distribution of the ψ' shown in Fig. 12a illustrates that a wavepacket propagates zonally along the jet as in Naoe et al., while the ψ' field of Fig. 7 shows both zonal and meridional propagation. However, a closer inspection of Fig. 12a reveals a hint of meridional propagation of anomalies. A slight southward propagation between 90°E and 150°E and a northward propagation

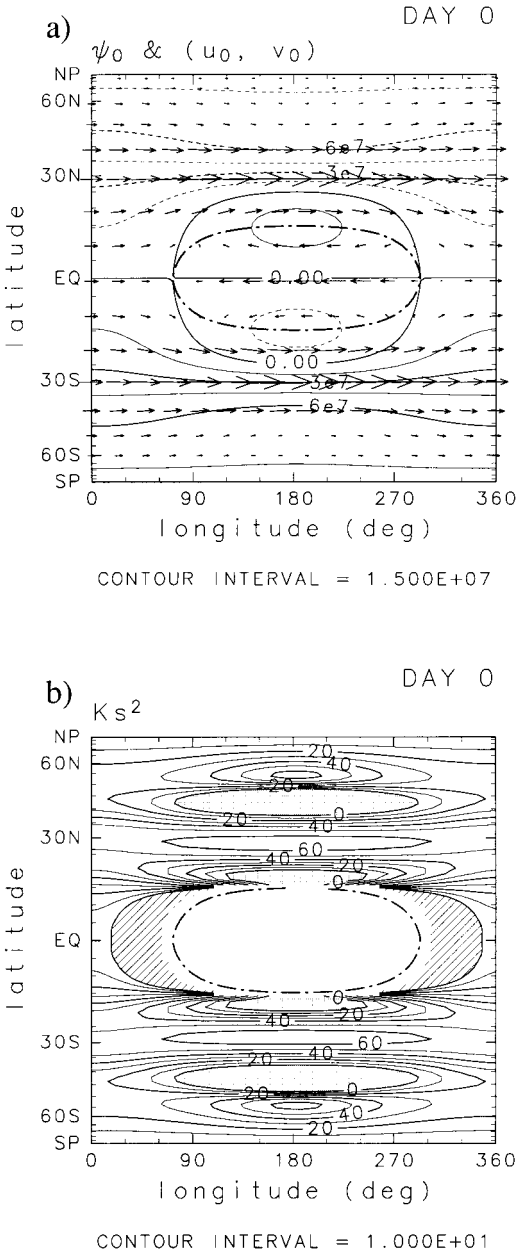

Fig. 11. As in Fig. 2 except for the basic flow of Naoe et al. (1997).

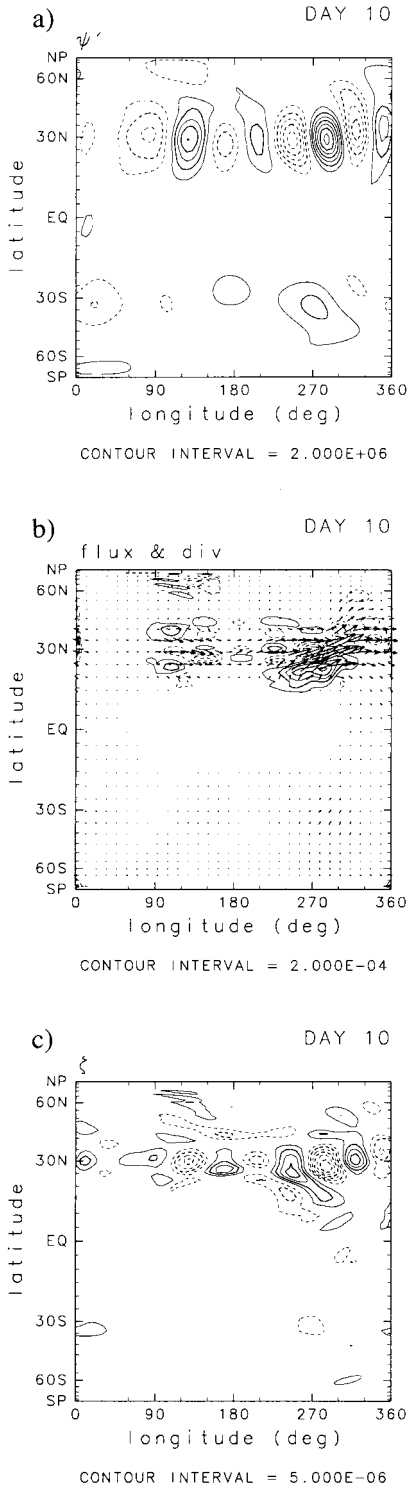

Fig. 12. Distribution of (a) the perturbation streamfunction, (b) wave-activity flux (arrows) and its divergence (contours), and (c) the perturbation relative vorticity are shown. The Panels (b)–(c) show snapshots at day 10.

between 180°E and 270°E are exhibited. The phase lines of anomalies vary correspondingly from NE–SW to NW–SE. This slight meridional propagation suggests that a reflection occurs at the southern flank of the jet near 180°E. In Fig. 12b, an absorption of wave activity occurs in the region to the west of the 180°E meridian, which may act to weaken the wavepacket. As a result, the amplitude of ψ' anomalies near this meridian is somewhat smaller than others. The meridional location of the reflection exists in the region with small K_s in Fig. 11b. Moreover, ζ' anomalies do not seem to be advected in Fig. 12c in contrast to that in Fig. 7. Therefore, it is probable that a low-latitude reflection occurred, by contrast to case 3, at the turning latitudes.

Naoe et al. (1997) found that the wave amplification near the jet exit region is mainly due to the barotropic KE conversion $-u'v'a^{-1}\,\partial\bar{u}_0/\partial\phi$ and that this amplification is possible without barotropic instability. In Figs. 12a, b, the NW–SE tilt on the southern flank of the jet exit implies an occurrence of a strong positive barotropic KE conversion, associated with the negative correlation between u' and v'. The mechanism of the jet exit wave amplification is due to the tilted phase lines caused by the anticyclonic flow in this case as well as in case 3. In other words, a tilt of phase lines of the reflected waves acts to amplify the wave amplitude in the jet exit region. The amplification of the wave amplitude is also seen in the distribution of wave-activity flux shown in Fig. 12c. There is a convergence centring near 25°N, 150°E. Northeastward wave-activity flux is emanating from divergence centring near 20°N, 270°E. This divergence–convergence pattern is reminiscent of Fig. 8a.

5. Concluding remarks

A simplified model should retain the most important features of the original problem. A treatment with monochromatic wave propagation in a zonal mean flow is the simplest possible one

for considering meridional wave propagation. The SWW solution is based on the assumption that the basic flow is exactly zonally-uniform. However, in the real atmosphere, the flow is, more or less, zonally-varying. In the present numerical experiments conducted for such a basic flow, the SWW solution could not be realized. In the SWW solution, to avoid the singularity of the linearized vorticity equation at the critical latitude, the nonlinear terms are considered. In a zonally-varying basic flow, by contrast, the zonally-varying component may remove the singularity of the linearized vorticity equation. In this sense, a very special situation was considered when obtaining the SWW solution. The present results confirm the primary importance of passive advection of vorticity by the zonally-varying basic flow even near the critical line. Hence, it is suggested that the SWW solution is hardly realized in the real tropospheric situation. There are certain upper tropospheric phenomena in which nonlinearity is of primary importance as noted in the Introduction. It is interesting to examine whether linearity or nonlinearity is important in the upper troposphere. This topic will be discussed elsewhere.

5. Acknowledgements

The authors wish to acknowledge very useful conversation with Prof. Maslowe at the Rossby-100 symposium and helpful comments made by Dr H. Nakamura. We thank Editor Dr Lejenäs and the anonymous reviewers for valuable comments. One of the authors (T.E.) is supported by the JSPS Research Fellowship. The figures were produced with the GFD-DENNOU Library.

REFERENCES

Brunet, G. and Haynes, P. H. 1996. Low-latitude reflection of Rossby wave trains. *J. Atmos. Sci.* **53**, 482–496.

Brown, S. N. and Stewartson, K. 1979. On the secular stability of a regular Rossby neutral mode. *Geophys. Astrophys. Fluid Dyn.* **14**, 1–18.

Campbell, L. J. and Maslowe, S. A. 1998. Forced Rossby wave packets in barotropic shear flows with critical layers. *Dyn. Atmos. and Oceans* **28**, 9–37.

Enomoto, T. and Matsuda, Y. 1999. Numerical experiments on the behaviour of Rossby waves in the critical layer. *Fluid Dyn. Res.*, in press.

Hoskins, B. J. and Ambrizzi, T. 1993. Rossby wave propagation on a realistic longitudinally varying flow. *J. Atmos. Sci.* **50**, 1661–1671.

McIntyre, M. E. and Palmer, T. N. 1983. Breaking planetary waves in the stratosphere. *Nature* **305**, 593–600.

McIntyre, M. E. and Shepherd, T. G. 1987. An exact local conservation theorem for finite-amplitude disturbances to non-parallel shear flows, with remarks on Hamiltonian structure on Arnold's stability theorems. *J. Fluid Mech.* **181**, 527–565.

Merkine, L.-O. and Bar-Server. Y. 1989. Local instabilities of weakly non-parallel large-scale flows: marginal stability and non-parallel critical layers. *Geophys. Astrophys. Fluid Dyn.* **47**, 93–130.

Nakamura, H. 1994. Rotational evolution of potential vorticity associated with a strong blocking configuration over Europe. *Geophys. Res. Lett.* **21**, 2003–2006.

Nakamura, H., Nakamura, M. and Anderson, J. L. 1997. The role of high- and low-frequency dynamics in blocking formation. *Mon. Wea. Rev.* **125**, 2074–2093.

Naoe, H., Matsuda, Y. and Nakamura, H. 1997. Rossby wave propagation in idealized and realistic zonally varying flows. *J. Meteor. Soc. Japan* **75**, 687–700.

Postel, G. A. and Hitchman, M. H. 1999. A climatology of Rossby wave breaking along the subtropical tropopause. *J. Atmos. Sci.* **56**, 359–373.

Plumb, R. A. 1985. On the three-dimensional propagation of stationary waves, *J. Atmos. Sci.* **42**, 217–229.

Simmons, A. J., Wallace, J. M. and Branstator, G. W. 1983. Barotropic wave propagation and instability, and atmospheric teleconnection patterns. *J. Atmos. Sci.* **40**, 1363–1392.

Stewartson, K. 1978. The evolution of the critical layer of a Rossby wave. *Geophys. Fluid Dyn.* **9**, 185–200.

Takaya K. and Nakamura, H. 1997. A formulation of a wave activity flux of stationary Rossby waves on a zonally-varying basic flow. *Geophys. Res. Lett.* **24**, 2985–2988.

Warn, T. and Warn, H. 1978. The evolution of a nonlinear Rossby wave critical level. *Stud. Appl. Math.* **59**, 37–71.

Waugh, D. W., Polvani, L. M. and Plumb, R. A. 1994. Nonlinear, barotropic response to a localized topographic forcing: formation of a tropical surf zone and its effect on interhemispheric propagation. *J. Atmos. Sci.* **51**, 1401–1416.

Webster, P. J. and Holton, J. R. 1982. Cross-equatorial response to middle latitude forcing in zonally varying basic state. *J. Atmos. Sci.* **39**, 722–733.

Webster, P. J. and Chang, H.-R. 1997. Atmospheric wave propagation in heterogeneous flow: basic flow controls on tropical–extratropical interaction and equatorial wave modification. *Dyn. Atmos. Oceans* **27**, 91–134.